Enhanced Imaging Algorithm for Scanning Laser Polarimetry with Variable Corneal Compensation

Nicolaas J. Reus,[1] *Qienyuan Zhou,*[2] *and Hans G. Lemij*[1]

Purpose. To describe and investigate a method of improving assessment of retinal nerve fiber layer (RNFL) morphology with scanning laser polarimetry (SLP) with variable corneal compensation (VCC).

Methods. By neutralizing anterior segment birefringence with a variable compensator, the current VCC method allows direct measurement of RNFL retardation. In the new method, enhanced corneal compensation (ECC), the variable compensator was set to introduce a "bias" birefringence. This bias was removed mathematically for each individual pixel to produce the RNFL image. In 177 eyes of healthy subjects, patients with glaucoma, and subjects with ocular hypertension, retardation images were obtained with both VCC and ECC.

Results. In the tested eyes, images obtained with ECC showed the expected RNFL appearance better than those obtained with VCC. In addition, the typical scan score, which quantifies the amount of atypia, was higher with ECC than with VCC. The amount of residual anterior segment birefringence dropped significantly with ECC in the various groups. Measurements of peripapillary RNFL retardation showed reduced temporal and nasal values with ECC, whereas superior and inferior values were not significantly different between VCC and ECC. The dynamic range appeared to have increased with ECC. The accuracy of the TSNIT (temporal, superior, nasal, inferior, temporal) average and inferior average for detecting glaucoma was higher with ECC than with VCC.

Conclusions. RNFL morphology may be better assessed with the presented ECC method than with standard VCC. ECC may be implemented in the current VCC systems by means of a software upgrade. It may enhance the clinical utility of the GDx VCC in glaucoma management. (*Invest Ophthalmol Vis Sci.* 2006;47:3870–3877) DOI:10.1167/iovs.05-0067

Scanning laser polarimetry (SLP) has been developed for detecting and monitoring glaucoma, an acquired progressive optic neuropathy with atrophy of retinal ganglion cells and their axons.[1] SLP is based on the presumed form birefringence of the microtubules in the retinal nerve fiber layer (RNFL).[2] Their parallel arrangement results in a change in the retardation of passing polarized light. In SLP, the back of the eye is scanned with a polarized laser beam and the retardation of the backscattered light that has double passed the RNFL is determined. The amount of retardance exhibited by the RNFL is proportional to its thickness,[3] although the slope of the linear relationship may vary around the optic nerve head.[4,5]

Two structures in the anterior segment (i.e., the cornea and, to a lesser extent, the lens) are also birefringent. When assessing RNFL retardation, anterior segment retardation must be neutralized.[6,7] Earlier commercial SLPs were equipped with a fixed corneal compensator (FCC) that cancelled a fixed amount of birefringence reflecting the median magnitude and axis of anterior segment birefringence in the general population.[6] Recently, SLP with variable corneal compensation (VCC) was introduced, which allows eye-specific compensation of anterior segment birefringence.[8] This technique is implemented in the commercially available GDx VCC (Carl Zeiss Meditec, Inc., Dublin, CA). SLP-VCC has been shown to allow a more accurate assessment of RNFL morphology[9] with a higher diagnostic accuracy for detecting glaucoma[10,11] than SLP-FCC provides.[12] Further, measurements with SLP-VCC have been shown to correlate well with functional measurements by standard automated perimetry.[13,14]

Typically, in healthy subjects, larger amounts of retardation are apparent next to the blood vessels superior and inferior to the optic nerve head (ONH; e.g., Fig. 1A). The amount of retardation decreases with increasing distance from the ONH. In glaucomatous eyes, the loss of nerve fibers is visible as a localized and/or diffuse decrease in the amount of retardation (e.g., Fig. 1B). In approximately 7% of subjects, atypical patterns of increased retardation may be apparent in images obtained with SLP-VCC (e.g., Fig. 1C, 1D, left).[10] The atypical retardation pattern has been characterized as irregular patches of elevated retardation values that do not match the expected retardation distribution based on the retinal nerve fiber layer.[15] Thus, the RNFL in these so-called atypical scans may be difficult to interpret. The source of this aberrant retardation is unknown, although it appears to occur more frequently in eyes with lightly pigmented fundi, in myopes, and in eyes of elderly subjects in which the signal-to-noise ratio of the SLP images is relatively poor.[10]

Although compensation of anterior segment birefringence in the individual eye seems to be adequate with SLP-VCC in general, a small amount of residual anterior segment birefringence can be observed in some eyes (e.g., Fig. 1E, left), which may lead to erroneous measurements of the RNFL.[9]

Both atypical retardation patterns and residual anterior segment birefringence adversely affect the accuracy of RNFL assessment with SLP. In this article, we present a method that minimizes atypical retardation patterns and residual anterior segment birefringence, which may improve the accuracy of RNFL assessment in affected eyes. We investigated this new method in healthy eyes, glaucomatous eyes, and eyes with ocular hypertension.

From the [1]Glaucoma Service, The Rotterdam Eye Hospital, Rotterdam, The Netherlands; and [2]Carl Zeiss Meditec, Inc., Dublin, California.

Supported by The Rotterdam Eye Hospital Research Foundation, Rotterdam, The Netherlands; Stichting Glaucoomfonds, Leiden, The Netherlands; and Laser Diagnostic Techologies (now Carl Zeiss Meditec).

Submitted for publication January 19, 2005; revised June 8 and October 27, 2005, and March 24, May 18, and May 30, 2006; accepted July 24, 2006.

Disclosure: **N.J. Reus**, Laser Diagnostic Technologies, Inc. (now Carl Zeiss Meditec, Inc.) (F); **Q. Zhou**, Carl Zeiss Meditec, Inc., Dublin, CA (E); **H.G. Lemij**, Laser Diagnostic Technologies, Inc. (C, F)

The publication costs of this article were defrayed in part by page charge payment. This article must therefore be marked "*advertisement*" in accordance with 18 U.S.C. §1734 solely to indicate this fact.

Corresponding author: Nicolaas J. Reus, The Rotterdam Eye Hospital, PO Box 70030, 3000 LM Rotterdam, The Netherlands; reus@eyehospital.nl.

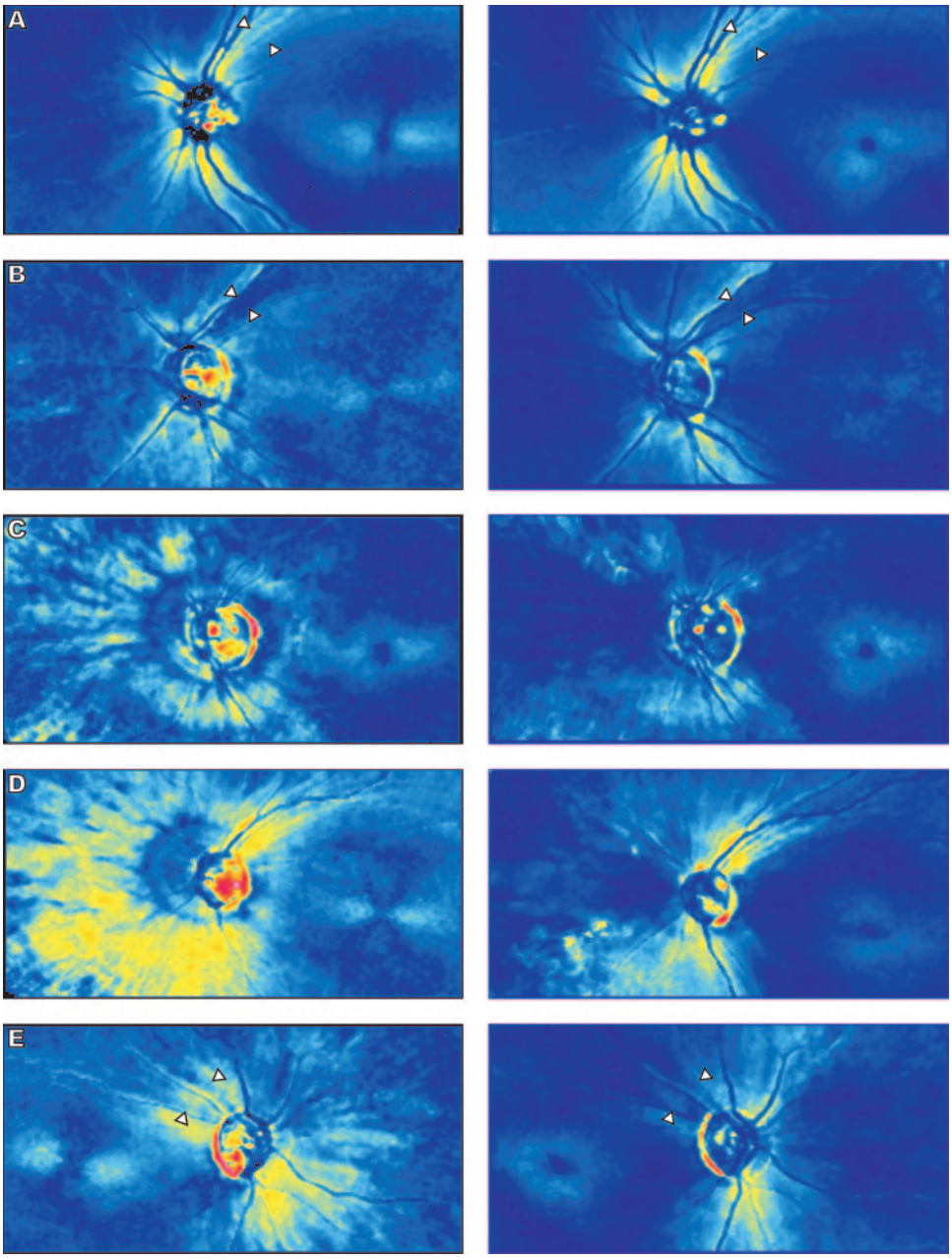

FIGURE 1. Retardation images of four left eyes and one right eye with standard VCC (*left*) and ECC (*right*). Brighter colors represent a thicker RNFL and darker colors a thinner RNFL. (**A**) A healthy eye (MD, 0.45 dB; PSD, 1.19 dB); residual retardation was 8 nm for VCC and 2 nm for ECC. The typical scan score was 99 and 100 for VCC and ECC, respectively. (**B**) A glaucomatous eye (MD, −6.19 dB; PSD, 8.8 dB); residual retardation was 5 nm for VCC and 1 nm for ECC. The typical scan score was 89 and 100 for VCC and ECC, respectively. (**C**) A glaucomatous eye (MD, −20.55 dB; PSD, 10.18 dB); residual retardation was 5 nm for VCC and 1 nm for ECC. The typical scan score was 45 and 100 for VCC and ECC, respectively. (**D**) A glaucomatous eye (MD, −3.04 dB; PSD, 6.14 dB); residual retardation was 6 nm for VCC and 0 nm for ECC. The typical scan score was 37 and 100 for VCC and ECC, respectively. (**E**) A glaucomatous right eye (MD, −11.69 dB; PSD, 13.66 dB); residual retardation was 12 nm for VCC and 0 nm for ECC. The typical scan score was 59 and 100 for VCC and ECC, respectively. With VCC, the large amount of residual anterior segment birefringence in the macular region had an axis of 23° nasally downward. The RFNL appeared to be rotated in the same direction. With ECC, the apparent distortion of the RNFL measurement had disappeared.

METHODS

Subjects

One hundred and seventy-seven subjects (29 healthy subjects, 70 patients with glaucoma, and 78 subjects with ocular hypertension) were recruited consecutively for the present study between February and July 2004 at The Rotterdam Eye Hospital. The research adhered to the tenets of the Declaration of Helsinki. The institutional human experimentation committee approved the research, and informed consent was obtained from the subjects after explanation of the nature and possible consequences of the study.

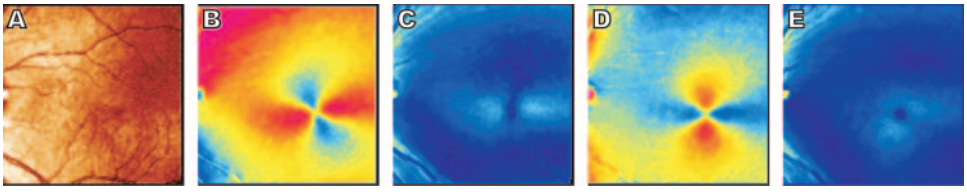

FIGURE 2. Macular images of a healthy subject's left eye. (**A**) Reflection image. (**B**) Retardation image without any compensation of anterior segment birefringence (50 nm and 19.6° nasally downward [ND]). (**C**) Retardation image with standard VCC compensation (13 nm and −78.3° ND). (**D**) Retardation image with artificially induced bias (27 nm and 82.2° ND). (**E**) Retardation image with anterior segment compensation by the ECC method (2 nm and 50.5° ND). Note that residual birefringence is less with ECC than with VCC.

All subjects were measured with standard automated perimetry (SAP) by means of the Humphrey Field Analyzer II (Carl Zeiss Meditec, Inc., Dublin, CA) 24-2 full threshold (FT) or Swedish Interactive Threshold Algorithm (SITA)-Standard test program. All visual fields were reliable. Reliability criteria applied were fixation losses <25% and false-positive and -negative response rates ≤20% for the FT test paradigm and ≤7% for the SITA-Standard test program. In glaucomatous eyes with advanced field loss, higher false-negative response rates were accepted: up to 33% for the FT paradigm and up to 12% for the SITA-Standard paradigm.

All healthy subjects had normal visual fields with SAP (i.e., a Glaucoma Hemifield Test (GHT) result within normal limits) and no nerve fiber bundle visual field defects in the total and/or pattern deviation probability plots. In addition, subjects were of white ethnic origin and had a visual acuity of 20/40 or better. None had a significant history of ocular disease, a history of intraocular surgery (except for any uncomplicated cataract surgery), relatives in the first and/or second degree with glaucoma, any significant coexisting diseases, or systemic diseases with possible ocular involvement, such as diabetes mellitus. Furthermore, slit lamp examination was unremarkable; they had healthy-looking optic discs (no diffuse or local rim thinning and no optic disc hemorrhages), an IOP of 21 mm Hg or less in both eyes, and open angles on gonioscopy. Their mean deviation (MD) and pattern standard deviation (PSD) were 0.27 ± 1.02 dB and 1.69 ± 0.51 dB (mean ± SD), respectively.

Patients with glaucoma had a glaucomatous appearance of at least one of their optic discs (with notching or thinning of the neuroretinal rim), a corresponding nerve fiber bundle visual field defect with SAP and open angles by gonioscopy. Visual field defects had to be confirmed on at least one separate examination. All patients with glaucoma were of white ethnic origin and had a visual acuity of 20/40 or better. Patients with any significant coexisting diseases other than glaucoma; systemic diseases with possible ocular involvement, such as diabetes mellitus; or a history of intraocular surgery (except for any uncomplicated cataract or glaucoma surgery) were excluded. The MD and PSD were −12.15 ± 8.07 (range, −30.40–0.61) and 9.25 ± 3.66 dB, respectively.

All subjects with ocular hypertension had an IOP of ≥22 mm Hg and ≤32 mm Hg and normal visual fields on at least two separate occasions. The appearance of the optic disc was not a selection criterion. All subjects with ocular hypertension were of white ethnic origin and had a visual acuity of 20/40 or better. Patients with a history of intraocular surgery (except for any uncomplicated cataract surgery), any significant coexisting diseases, or systemic diseases with possible ocular involvement, such as diabetes mellitus, were excluded. Their MD and PSD were 0.44 ± 1.28 and 1.68 ± 0.57 dB, respectively.

Only one eye was randomly selected for analysis in the present study if both were eligible.

The age of the healthy subjects, patients with glaucoma, and subjects with ocular hypertension was 60 ± 13, 68 ± 9, and 63 ± 10 years (mean ± SD), respectively. The difference in age between the various groups was statistically significant (one-way ANOVA, $P = 0.002$). In 13 (45%) of 29 healthy subjects, 33 (47%) of 70 with glaucoma, and 39 (50%) of 78 with ocular hypertension, the right eye was used for analysis. Twelve (41%) of the 29 healthy subjects, 37 (53%) of the 70 with glaucoma, and 43 (55%) of the 78 with ocular hypertension were men.

SLP Measurements

SLP measurements were performed with a commercially available GDx VCC (software version 5.4.0; Carl Zeiss Meditec, Inc., Dublin, CA). The GDx VCC used a near infrared laser beam with a wavelength of 785 nm to scan the ocular fundus. The field of view was 40° horizontally × 20° vertically at a density of 256 × 128 pixels. The scanned area included the papillary and the macular regions of the eye. The GDx VCC produced a reflection image that was generated from light reflected from the fundus of the eye. In addition, it produced a retardation image that had been constructed from the 32,768 (256 × 128) individual retardation values. The amount of retardation was displayed as apparent RNFL thickness (in micrometers) based on a conversion factor of 0.67 nm/μm.[16] The GDx VCC was equipped with a variable corneal compensator that consisted of two identical linear retarders in rotating mounts so that both the retardation and axis of the unit could be adjusted. To measure an individual's eye polarization axis and magnitude of the cornea (and the lens), an SLP image of the macula (Fig. 2A) was acquired with the retardation of the compensator set to zero. The combination of the birefringence of the radially oriented axons of the photoreceptors that constitute Henle's fiber layer in the macula and the birefringence of the anterior segment resulted in a bow-tie like retardation pattern in the macula (Fig. 2B). One of two dedicated algorithms incorporated into the GDx VCC (i.e., the "bow-tie" method and the "screen" method), determined the magnitude and axis of anterior segment birefringence from the macular retardation profile. These algorithms have been described in detail elsewhere.[8,16,17] In short, the bow-tie method calculated the anterior segment birefringence from the macular retardation profile obtained at a locus of points along a circle centered on the fovea.[8] The screen method averaged the signals from the parallel channel and the crossed channel over a large square area of the macula centered on the fixation target, to extract the anterior segment birefringence.[16] Although the bow-tie method works well in eyes with normal macula, the screen method is more robust in eyes with macular disease and a damaged Henle's fiber layer.[17]

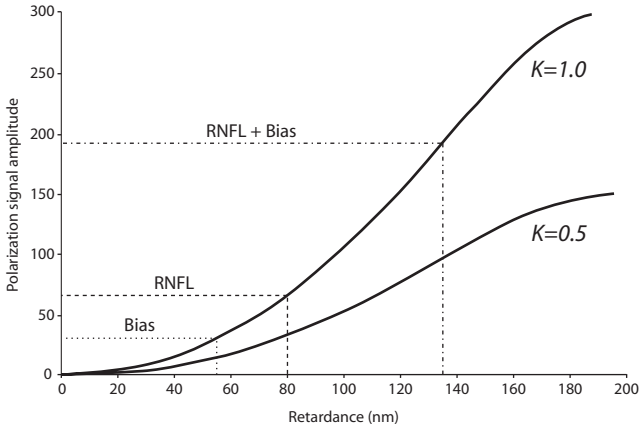

FIGURE 3. Plot of polarization signal amplitude versus retardation for different degrees of normalized polarization maintaining fundus reflectance (*K*).

In the currently implemented VCC technique, the compensator was automatically adjusted to neutralize the eye's anterior segment birefringence based on the measured values with the bow-tie method. The eye was then scanned with individualized compensation to measure the amount of retinal retardation. With anterior segment birefringence compensated, the retardation pattern in the macular region should exhibit a uniform and weak retardation pattern with a cross- or donut-shaped distribution (Fig. 2C). As an alternative to the existing VCC method, a new software method, enhanced corneal compensation (ECC; Carl Zeiss Meditec, Inc.), was developed that requires no hardware modification to the GDx VCC system and provides individualized corneal compensation with enhanced SLP measurement sensitivity. The rationale of this technique is as follows: The sensitivity of SLP to measuring small differences in retardation ultimately depends on the ability to detect small differences in polarization signal amplitude. SLP sensitivity (the slope of the curve) is inherently low at low retardation values, as shown in Figure 3. Depolarization or reduction in reflected light intensity results in a lower-intensity curve and proportionally decreased sensitivity, as illustrated with the curves for $K = 1.0$ and $K = 0.5$, where K represents the normalized polarization main-

TABLE 1. Typical Scan Scores in SLP Measurements

	VCC Method	ECC Method	*P*
Normal	89.0 ± 14.8 (50–100)	99.3 ± 1.8 (92–100)	0.001
Glaucoma	71.2 ± 28.6 (0–100)	97.8 ± 6.1 (69–100)	<0.001
Ocular hypertension	85.9 ± 19.1 (19–100)	99.9 ± 0.6 (95–100)	<0.001

Range, 0–100. VCC and the ECC methods were used in healthy, glaucomatous, and ocular hypertensive eyes. Data are expressed as the mean score ± SD (range). Differences were tested for statistical significance with a paired *t*-test.

taining fundus reflectance. Low sensitivity makes the retardation measurement susceptible to optical noise (e.g., stray light) and electronic noise (e.g., noise and digitization error). The principle of the new method, illustrated in Figure 3, was to superimpose RNFL birefringence onto a large, known birefringence ("bias retarder"). The bias retarder was formed by the combination of the variable compensator and the anterior segment. Rather than adjusting the VCC to neutralize the anterior segment birefringence, the compensator was adjusted so that the combination had a retardation of approximately 55 nm and a slow axis close to vertical. The bias retarder therefore shifted the retardation measurement into a more sensitive region (Fig. 3).

With ECC, SLP measured an amount of retardation that was higher than retinal retardation alone (Fig. 2D). The birefringence, induced by the bias retarder, was determined from the macular region with the screen method described earlier. Based on Mueller calculus for a double-pass SLP system, the retinal retardation was mathematically extracted from the total retardation image based on knowledge of the bias retarder retardation and axis, as well as knowledge of the point-by-point total retardation and axis.[18] Successful removal of bias retardation from the final retinal retardation image was evident from the uniform retardation pattern in the macula (Fig. 2E).

Three trained and experienced technicians performed the GDx VCC measurements in both eyes of all subjects. Pupils of subjects were undilated, and the room lights were left on. The spherical equivalent refractive error of each eye was entered into the software to allow the GDx VCC to focus on the retina. If necessary, the focus was adjusted manually in 0.25-D steps. For each subject, anterior segment birefringence was assessed, after which images were obtained from both eyes with VCC first and with ECC second. Subjects were asked to keep their heads positioned on the GDx VCC system's face mask between acquisitions. To maintain the same orientation of the slow axes of the birefringent structures in the eye to that of the instrument's compensator, the operator saw to it that patients had their heads in the same position during all measurements.

All accepted scans were of high quality (i.e., with a centered optic disc, well-focused, evenly illuminated throughout the image, and without any motion artifacts). No images were excluded from analysis that were flagged by the GDx VCC software as "Results may not be compatible with normative database." The software flags an image as such when the typical scan score is 25 or lower. The typical scan score (range, 0–100) is a proprietary measure provided by the GDx VCC software, which indicates whether the observed retardation pattern is typical of the human healthy or glaucomatous RNFL. In scans that display an atypical pattern of retardation (e.g., Figs. 1C, 1D, left), the typical scan score is lower. Similar to the nerve fiber indicator (NFI) parameter, the typical scan score is the output of a machine learning classifier based on a support vector machine. The exact calculation of this parameter is unknown. However, other groups have used this parameter to show that the typical scan score parameter is highly predictive of the presence of atypical birefringence patterns.[19]

Residual anterior segment birefringence was assessed in images obtained with VCC and ECC by determining the amount of retardation in the macular region with the bow-tie method.

Data Analysis

The margin of the optic disc was manually marked with an ellipse in the reflection image of the fundus. The GDx VCC software positioned a circular band, 8 pixels wide (~0.4 mm in an emmetropic eye) and with an inner diameter of 54 pixels (~2.5 mm in an emmetropic eye), centered on the center of the ellipse. The instrument processed the retardation values within this band to give 256 values evenly distributed along the circle. These values were subsequently grouped into 64 sectors and exported by the software. The measurement band was divided into four sectors: temporal (extending from 335°–24°, relative to the temporal meridian), superior (25°–144°), nasal (145°–214°), and inferior (215°–334°). Based on the retardation values within this band, we determined the average amount of retardation in all sectors and in the temporal, superior, nasal, and inferior regions: TSNIT average, temporal average, superior average, nasal average, and inferior average. In addition, we calculated the standard deviation of the mean amount of retardation beneath the entire measurement band (TSNIT SD) and determined the peak-to-trough values in the TSNIT plot. Furthermore, we determined the minimum amount of retardation in the temporal and nasal regions: temporal minimum and nasal minimum, respectively.

To investigate whether the range in measurements had increased with ECC compared with VCC, we identified, for the superior and inferior regions separately, 10% of healthy eyes with the largest amount of retardation by ECC and 10% of glaucomatous eyes with the smallest amount of retardation by ECC. For both VCC and ECC, we averaged the amounts of retardation in each group. We then calculated the differ-

TABLE 2. Corneal Polarization Magnitude

	CPM without Compensation	CPM, Residual		*P*
		VCC Method	ECC Method	
Normal	36.6 ± 13.0 (7–64)	6.5 ± 2.7 (1–11)	1.9 ± 1.9 (0–8)	<0.001
Glaucoma	38.6 ± 14.1 (2–75)	6.4 ± 3.1 (0–18)	1.8 ± 1.4 (0–6)	<0.001
Ocular hypertension	39.7 ± 15.2 (1–67)	6.1 ± 2.9 (1–21)	1.6 ± 1.3 (0–5)	<0.001

Data are expressed as mean micrometers ± SD (range) of CPM and were collected from healthy, glaucomatous, and ocular hypertensive eyes. CPM was determined with correction by a variable corneal compensator with the VCC and ECC methods. Differences in residual CPM with VCC and ECC were tested for statistical significance with a paired *t*-test.

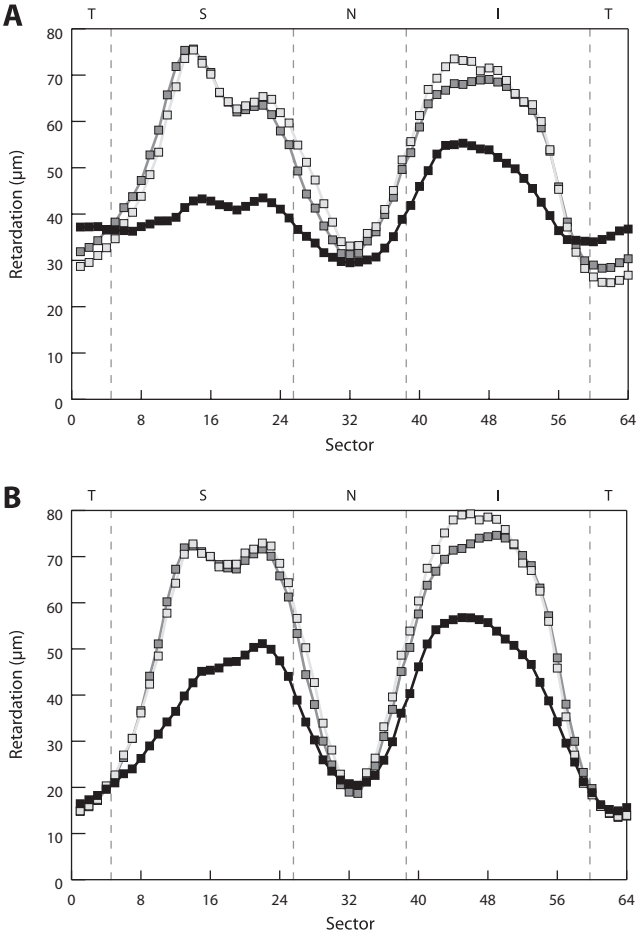

FIGURE 4. Peripapillary retinal nerve fiber layer retardation measured with scanning laser polarimetry with variable corneal compensation (VCC; **A**) and with ECC (**B**) in healthy eyes (□), eyes with ocular hypertension (▨), and glaucomatous eyes (■). T, temporal; S, superior; N, nasal; I, inferior.

ences in the amount of retardation between the healthy eyes and the glaucomatous eyes for VCC and ECC separately.

Furthermore, we determined the accuracy of SLP-VCC and SLP-ECC for discriminating between healthy and glaucomatous eyes by calculating the areas under the receiver operating characteristic (ROC) curves (AUCs) for four clinically used parameters (i.e., TSNIT average, superior average, inferior average, and TSNIT SD) obtained with VCC and with ECC. The 95% confidence intervals (CIs) for the AUCs were calculated as the point estimates of the AUC ± 1.96 · SE. Differences in AUCs of parameters obtained with VCC and ECC were tested for statistical significance with the paired samples test described by DeLong et al.[20]

We used paired and unpaired *t*-tests to evaluate differences in measurements within and between groups, respectively. In the present study, a P value of <0.05 was considered statistically significant. For paired comparisons, the α was adjusted to the number of comparisons within each analysis with the Bonferroni correction, to allow for multiple testing. Statistical analyses were performed using a computer (SPSS for Windows; release 12.0.1, 2003; SPSS Inc., Chicago, IL).

RESULTS

Figure 1 shows five examples of retardation images acquired with standard VCC (left) and with ECC (right); the peripapillary and the macular regions are displayed. These examples illustrate that the retardation images taken with ECC showed the expected RNFL appearance much better than images acquired with VCC (e.g., Fig. 1B, cf. right and left panels). The typical scan score was significantly higher ($P \leq 0.001$; $\alpha = 0.017$, three comparisons) for images with the ECC method than with the VCC method in all subjects (Table 1). This is illustrated in Figures 1C and 1D, in which atypical retardation patterns were less pronounced in images acquired with ECC (right; higher typical scan score parameter values) compared with VCC (left; lower typical scan score parameter values). The morphology of the RNFL looked similar in images obtained with either VCC or ECC in almost every eye. For example, in Figure 1A, several slitlike defects superotemporal to the optic disc were equally well visible with both methods. Similarly, the localized RNFL defects superotemporal to the optic disc in Figures 1B and 1E were marked with either method.

Images obtained with ECC contained significantly ($P < 0.001$; $\alpha = 0.017$, three comparisons) less residual anterior segment birefringence than did images obtained with VCC (Table 2, Fig. 1, cf. macular regions in the left and right panels). Images taken with VCC often showed a horizontally placed bow-tie (Fig. 1, left). The mean ± SD axis of this residual anterior segment birefringence in healthy, ocular hypertensive, and glaucomatous eyes was 8° ± 21° nasally downward. In images with a large residual amount of birefringence, the morphology of the RNFL sometimes appeared to be rotated (e.g., Fig. 1E, left panel).

Peripapillary retardation values measured with VCC and ECC are presented in Figures 4A and 4B, respectively. The shapes of these so-called TSNIT graphs were markedly different

TABLE 3. Parameters Describing SLP Measurements with the VCC and ECC Method

	Normal			Glaucoma			Ocular Hypertension		
Parameter	**VCC**	**ECC**	***P***	**VCC**	**ECC**	***P***	**VCC**	**ECC**	***P***
TSNIT average	52.7 ± 6.0	50.2 ± 5.2	<0.001	41.1 ± 8.2	36.9 ± 6.1	<0.001	52.3 ± 5.3	48.9 ± 4.6	<0.001
Temporal average	28.9 ± 7.9	16.7 ± 5.1	<0.001	36.4 ± 12.5	17.3 ± 5.1	<0.001	32.3 ± 9.8	16.4 ± 3.7	<0.001
Superior average	62.8 ± 8.0	62.9 ± 7.8	0.82	42.7 ± 9.2	42.9 ± 8.9	0.76	63.1 ± 7.8	62.6 ± 7.9	0.26
Nasal average	41.2 ± 7.0	32.8 ± 6.3	<0.001	32.6 ± 6.4	26.3 ± 6.5	<0.001	38.4 ± 8.9	29.9 ± 7.1	<0.001
Inferior average	59.6 ± 8.6	61.7 ± 8.3	0.012	46.5 ± 11.9	45.3 ± 9.4	0.18	58.0 ± 8.0	60.1 ± 6.7	<0.001
TSNIT SD	18.9 ± 3.7	24.5 ± 4.1	<0.001	11.9 ± 3.2	16.4 ± 3.9	<0.001	18.5 ± 4.2	23.9 ± 3.4	<0.001
Peak-to-trough	66.3 ± 10.5	75.5 ± 10.0	<0.001	45.6 ± 11.7	56.9 ± 12.6	<0.001	66.0 ± 12.0	75.2 ± 9.7	<0.001
Temporal minimum	22.9 ± 6.8	12.5 ± 4.5	<0.001	31.0 ± 11.6	13.2 ± 4.0	<0.001	25.8 ± 9.6	12.4 ± 3.2	<0.001
Nasal minimum	29.9 ± 7.1	17.8 ± 7.1	<0.001	25.5 ± 5.9	17.2 ± 7.1	<0.001	28.3 ± 9.1	16.2 ± 6.5	<0.001

Data are expressed as mean micrometers ± SD and were collected in healthy, glaucomatous, and ocular hypertensive eyes. Differences in measurements with VCC and ECC were tested for statistical significance with paired *t*-tests.

TABLE 4. Average Retardation in the Superior and Inferior Regions

	Superior Region				Inferior Region			
	VCC		ECC		VCC		ECC	
	Average	Δ	Average	Δ	Average	Δ	Average	Δ
Healthy	75.5	47.3	77.3	51.5	73.8	42.6	75.7	46.4
Glaucomatous	28.5		25.8		31.2		29.3	

Data were obtained with VCC and with ECC in the 10% of healthy eyes with the largest amount of retardation and in the 10% of glaucomatous eyes with the smallest amount of retardation. The difference (Δ) in retardation between the healthy and glaucomatous eyes is presented as well.

between the two methods. Statistically, TSNIT average, temporal average, nasal average, temporal minimum, and nasal minimum were significantly ($P \leq 0.001$, $\alpha = 0.006$, nine comparisons) lower with ECC than with VCC in all subjects (Table 3). TSNIT SD and the peak-to-trough values were significantly ($P < 0.001$, $\alpha = 0.006$, nine comparisons) higher with ECC than with VCC (Table 3), which was apparent as a larger modulation of the TSNIT graph with ECC (cf. Figs. 4B, 4A, respectively). The parameters' superior and inferior averages were not significantly ($P \geq 0.012$, $\alpha = 0.006$, nine comparisons) different between ECC and VCC in any of the tested groups, except for the inferior average in the subjects with ocular hypertension ($P < 0.001$, Table 3). This difference, however, was small (on average 2.1 μm).

The difference in the amount of retardation between healthy eyes with the largest amount of retardation and the glaucomatous eyes with the smallest amount of retardation are presented in Table 4. In both the superior and inferior regions, the range of measurements appeared larger for measurements with ECC than with VCC.

Of note, in images obtained with VCC, the average values in the temporal quadrant (temporal average) were significantly higher in glaucomatous eyes (36.6 μm) than in healthy eyes (28.6 μm; $P < 0.001$; cf. Fig. 4A, 4B). In images obtained with ECC, this difference was not statistically significant (glaucomatous eyes and healthy eyes: 17.3 μm and 16.0 μm, respectively; $P = 0.22$). In addition, the amount of retardation in the temporal region in healthy and ocular hypertensive eyes measured with VCC significantly ($P = 0.006$, $\alpha = 0.013$, four comparisons) correlated with the amount of residual anterior segment birefringence (Table 5). In the nasal region, this correlation was of borderline significance ($P = 0.016$, $\alpha = 0.013$, four comparisons). With ECC, no relationship was apparent between measured peripapillary retardation and residual anterior segment birefringence (Table 5). These data suggest that some of the differences between VCC and ECC were due to an artifactual increase in RNFL retardation in the temporal and nasal regions and a decrease in certain sectors of the superior and inferior regions caused by the compensation residual with VCC.

TABLE 5. Association between the Amount of Retardation in the Four Peripapillary Regions and the Residual Anterior Segment Birefringence

	CPM, Residual			
	VCC		ECC	
	ρs	*P*	ρs	*P*
Temporal average	0.26	0.006	−0.02	0.83
Superior average	−0.07	0.48	0.08	0.42
Nasal average	0.23	0.016	−0.04	0.71
Inferior average	−0.14	0.15	−0.17	0.077

Data are expressed as Spearman's rank correlation coefficient (ρs), and were measured by VCC and ECC in healthy and ocular hypertensive eyes.

The AUCs of the four clinically used parameters obtained with SLP-VCC and with SLP-ECC are presented in Table 6. The AUCs of the parameters TSNIT average and inferior average were significantly larger ($P = 0.004$ and $P = 0.002$, respectively; $\alpha = 0.013$, four comparisons) for measurements with ECC than with VCC. No statistically significant difference between measurements with VCC and ECC was found for the other two parameters.

DISCUSSION

We have presented a new method, ECC, that improves the signal-to-noise ratio of RNFL retardation measurements with SLP by shifting the measurements to a more sensitive detection range of the instrument. The shift is made by introducing a preset measurement bias that is mathematically removed from the measurements afterward. Measurements obtained with ECC appeared to represent the expected RNFL morphology better than or as well as those made with standard VCC. ECC can be implemented in the current GDx VCC (Carl Zeiss Meditec, Inc.) simply by a software upgrade.

With ECC, the typical scan score was higher than with VCC, suggesting that atypical retardation patterns were less pronounced in images obtained with ECC, which agrees with other reports.[15,21] As scans with an atypical retardation pattern may be difficult to interpret clinically, we suspect that more patients with glaucoma and those with suspected glaucoma may be assessed reliably with ECC. The origin of atypical scans is not yet fully understood. However, it appears to be associated with a low signal-to-noise ratio. In areas of low retardation (i.e., where the RNFL is thin), the measurements are susceptible to both optical and electronic noise. By introducing and later removing a preset measurement bias, the instrument's measurement sensitivity is enhanced, thereby reducing its susceptibility to such errors and perhaps explaining why atypical retardation is reduced with ECC.

By mathematically removing the induced bias in images obtained with this method, the residual of anterior segment birefringence compensation was also reduced with ECC compared with VCC. With VCC, the RNFL morphology appeared rotated in some eyes, probably due to the interaction between RNFL retardation and residual anterior segment retardation. In addition, the residual anterior segment birefringence in VCC images, with its mean axis close to the horizontal, artifactually increased retardation in the temporal and nasal parapapillary regions and reduced retardation in the superior and inferior

TABLE 6. Diagnostic Accuracy, Expressed as AUC

Parameters	VCC	ECC	Difference	*P*
TSNIT average	0.87 (0.035; 0.80–0.94)	0.96 (0.017; 0.93–1.00)	−0.09	0.004
Superior average	0.95 (0.019; 0.92–0.99)	0.98 (0.011; 0.96–1.00)	−0.03	0.062
Inferior average	0.81 (0.045; 0.72–0.89)	0.90 (0.031; 0.84–0.96)	−0.09	0.002
TSNIT SD	0.93 (0.026; 0.88–0.98)	0.93 (0.030; 0.87–0.99)	0	0.87

Data are expressed as the standard error (95% CI), for the listed parameters, to discriminate between healthy eyes and eyes with glaucoma.

regions where the nerve fiber bundles are nearly perpendicular to the slow axis of the compensation residual. Because the images were better compensated with ECC than with VCC, ECC may improve computer-assisted analysis of RNFL loss, such as the automated detection of localized RNFL defects,[22] which may aid clinicians in the interpretation of the polarimetry data.

With less residual anterior segment birefringence, ECC may also improve the instrument's accuracy for diagnosing and monitoring glaucoma. In fact, we showed that the diagnostic accuracy of the parameters TSNIT average and inferior average for discriminating between healthy eyes and eyes with glaucoma was higher in measurements with ECC than with VCC. As we presently included mostly patients with moderate to severe glaucoma, future studies may address whether the diagnostic accuracy of ECC is also improved over VCC in patients with mild glaucomatous damage. Of note, the AUCs that we found for VCC and ECC may both have been favorably biased by the statistically significant difference in age between healthy subjects and patients with glaucoma. Future studies are needed to determine the diagnostic accuracy in an age-matched population.

The SLP retardation measurement floor appeared to be lower with ECC than with VCC. Therefore, we think that the dynamic range of measurements may be larger with ECC. With a larger dynamic range, ECC SLP then may increase the ability to monitor patients with glaucoma over a longer time. The ability to monitor glaucomatous thinning of the RNFL over time also depends on the reproducibility of measurements and the sensitivity of a device in measuring small changes. Therefore, follow-up studies will have to be conducted, especially in eyes with more advanced RNFL loss, to show whether the detection of progressive damage has indeed improved with ECC.

With VCC, the temporal average was higher in glaucomatous eyes than in healthy ones, which was most likely due to measurement artifacts. In ECC, we found no difference in RNFL retardation between healthy and glaucomatous eyes in the nasal and temporal segments. One would have expected glaucomatous eyes to have a thinner RNFL in these regions as well, especially in eyes with advanced glaucoma. The source of this retardation, whether it is biological or artifactual, remains to be investigated. Alternative techniques, such as polarization-sensitive optical coherence tomography (PS-OCT)[4] may be used to provide additional insight. In addition, small atypical retardation patches remained in some images obtained with ECC (e.g., Fig. 1D), which should also be investigated in the future.

The dynamic range of the SLP system in the GDx VCC is a quarter of its laser's wavelength (i.e., approximately 195 nm) However, the maximum amount of retardation measured by the GDx VCC is 130 nm, which is a software-set limit. If in a given eye, the total amount of retardation induced by the RNFL and the 55-nm retardation bias were to exceed 130 nm, the measured values would be cropped at 130 nm. In such a case, measurement with the standard VCC method would be recommended. However, such cases are rarely observed. In addition, such an eye is unlikely to have a critically thinned RNFL.

In conclusion, ECC appears to yield improved SLP images of the RNFL, compared with VCC, which may allow clinicians a more accurate assessment of the retinal nerve fiber layer with the GDx VCC for diagnosing and monitoring glaucoma.

References

1. Quigley HA. Neuronal death in glaucoma. *Prog Retin Eye Res*. 1999;18:39–57.
2. Knighton RW, Huang X, Zhou Q. Microtubule contribution to the reflectance of the retinal nerve fiber layer. *Invest Ophthalmol Vis Sci*. 1998;39:189–193.
3. Weinreb RN, Dreher AW, Coleman A, et al. Histopathologic validation of Fourier-ellipsometry measurements of retinal nerve fiber layer thickness. *Arch Ophthalmol*. 1990;108:557–560.
4. Cense B, Chen TC, Park BH, Pierce MC, De Boer JF. Thickness and birefringence of healthy retinal nerve fiber layer tissue measured with polarization-sensitive optical coherence tomography. *Invest Ophthalmol Vis Sci*. 2004;45:2606–2612.
5. Huang XR, Bagga H, Greenfield DS, Knighton RW. Variation of peripapillary retinal nerve fiber layer birefringence in normal human subjects. *Invest Ophthalmol Vis Sci*. 2004;45:3073–3080.
6. Greenfield DS, Knighton RW, Huang XR. Effect of corneal polarization axis on assessment of retinal nerve fiber layer thickness by scanning laser polarimetry. *Am J Ophthalmol* 2000;129:715–722.
7. Weinreb RN, Bowd C, Greenfield DS, Zangwill LM. Measurement of the magnitude and axis of corneal polarization with scanning laser polarimetry. *Arch Ophthalmol*. 2002;120:901–906.
8. Zhou Q, Weinreb RN. Individualized compensation of anterior segment birefringence during scanning laser polarimetry. *Invest Ophthalmol Vis Sci*. 2002;43:2221–2228.
9. Reus NJ, Colen TP, Lemij HG. Visualization of localized retinal nerve fiber layer defects with the GDx with individualized and with fixed compensation of anterior segment birefringence. *Ophthalmology*. 2003;110:1512–1516.
10. Reus NJ, Lemij HG. Diagnostic accuracy of the GDx VCC for glaucoma. *Ophthalmology*. 2004;111:1860–1865.
11. Medeiros FA, Zangwill LM, Bowd C, Weinreb RN. Comparison of the GDx VCC scanning laser polarimeter, HRT II confocal scanning laser ophthalmoscope, and Stratus OCT optical coherence tomograph for the detection of glaucoma. *Arch Ophthalmol*. 2004;122:827–837.
12. Tannenbaum DP, Hoffman D, Lemij HG, et al. Variable corneal compensation improves discrimination between normal and glaucomatous eyes with the scanning laser polarimeter. *Ophthalmology* 2004;111:259–264.
13. Reus NJ, Lemij HG. The relationship between standard automated perimetry and GDx VCC measurements. *Invest Ophthalmol Vis Sci*. 2004;45:840–845.
14. Schlottmann PG, De Cilla S, Greenfield DS, Caprioli J, Garway-Heath DF. Relationship between visual field sensitivity and retinal nerve fiber layer thickness as measured by scanning laser polarimetry. *Invest Ophthalmol Vis Sci*. 2004;45:1823–1829.

15. Toth M, Hollo G. Enhanced corneal compensation for scanning laser polarimetry on eyes with atypical polarisation pattern. *Br J Ophthalmol*. 2005;89:1139–1142.
16. Zhou Q, Reed J, Betts RW, et al. Detection of glaucomatous retinal nerve fiber layer damage by scanning laser polarimetry with custom corneal compensation. *Proc SPIE Int Soc Opt Eng* 2003;4951: 32–41.
17. Knighton RW, Huang XR. Analytical methods for scanning laser polarimetry. *Opt Exp*. 2002;10:1179–1189.
18. Knighton RW, Zhou Q. New techniques. In: Iester M, Garway-Heath DF, Lemij HG, eds. *Optic Nerve Head and Retinal Nerve Fibre Analysis.* Savona, Italy: Dogma; 2005:117–119.
19. Bagga H, Greenfield DS, Feuer WJ. Quantitative assessment of atypical birefringence images using scanning laser polarimetry with variable corneal compensation. *Am J Ophthalmol* 2005;139: 437–446.
20. DeLong ER, DeLong DM, Clarke-Pearson DL. Comparing the areas under two or more correlated receiver operating characteristic curves: a nonparametric approach. *Biometrics*. 1988;44:837–845.
21. Sehi M, Guaqueta DC, Greenfield DS. An enhancement module to improve the atypical birefringence pattern using scanning laser polarimetry with variable corneal compensation. *Br J Ophthalmol.* Published online February 15, 2006.
22. Vermeer KA, Vos FM, Lemij HG, Vossepoel AM. Detecting glaucomatous wedge shaped defects in planimetrie images. *Med Image Anal*. 2003;7:503–511.